Int. J. Electrochem. Sci., 10 **(2015)** 1940 - 1952

International Journal of
ELECTROCHEMICAL
SCIENCE
www.electrochemsci.org

Design of a High Power Battery Based on an Analysis of Data Captured from a Commercial Hybrid Electric Vehicle Running at Operating-Mode Conditions

Daojun Yang[1,2], *Jinlong Xu*[2], *Xiaojian Jing*[2], *Ningning Wu*[2], *Wenhuai Tian*[1,*]

[1] School of Materials Science and Engineering, University of science and technology Beijing, Beijing, 100083, China
[2] CITIC Guoan Mengguli Power Science and Technology CO., LTD, Beijing, 102200, China
[*]E-mail: libydj@163.com

Received: 12 November 2014 / *Accepted:* 29 December 2014 / *Published:* 19 January 2015

The automotive industry requires electric vehicle battery systems to maintain specified performance for an 8 year life cycle. However, it has been shown for Li-ion batteries that the capacity loss after a 1 year operation is approximately 3%, and the power loss is approximately 8%. This is primarily due to battery internal resistance increasing over time caused by growth in SEI film thickness and a reduction in electrode adhesion. In this study, data were collected from a commercial hybrid electric vehicle battery system running at operating-mode conditions over a period of 1 year. In total, approximately 340,000 data samples were recorded. Of these data, about 92% discharge current was less than 50 A and the peak at 150 A; about 97% charge current was less than 75 A and the peak at 120 A. Based on an analysis of the collected data, a model simulating operating-mode performance was developed. The model addressed the three parameters - temperature, vibration and current. In order to better meet the requirement of commercial hybrid electric vehicles, a high performance 6 Ah high power battery was designed. The maximum charge and discharge current reached 180 A and 210 A, respectively. Using the developed simulation model, it can be shown that the 1-year discharge power loss of the battery is less than 3%, with negligible capacity degradation. It is therefore concluded that the 6Ah high power battery can meet the 8 year life cycle requirement of the automotive industry.

Keywords: commercial hybrid electric vehicle; high power battery; simulation operating-mode model; capacity loss; power loss

1. INTRODUCTION

Lithium-ion (Li-ion) batteries, increasingly being used in modern consumer electronics, are now also being targeted for use in automotives. In any application, not knowing a battery's rate of

capacity loss or useful life poses a significant business risk. For the automotive industry, knowing this information is critical and a pre-requisite for determining the performance and durability of the battery in applications.

Over the past few years there have been substantial efforts focused on the development of models to predict capacity and power degradation in Li-ion batteries [1–12]. Models have been developed to account for parameters known to be responsible for battery capacity degradation, such as parasitic side reactions [5,13,14], solid electrolyte interphase (SEI) formation [6], and resistance increase [1,10,15,16]. However, to validate these models, experimental data are required. To generate such data a systematic approach to data capture and model refinement is required.

Previous laboratory studies have been based on simulating operating mode conditions by varying temperature and current density. Initially the authors studied the performance of $LiMn_2O_4$/graphite batteries, simulating operating-mode conditions by varying vibrations and temperature [16]. But, in reality, when deployed in an automotive, batteries are subject to temperature shock, alternating currents, and vibration. Therefore, in order to better design automotive battery, reliable battery simulation models must address temperature shock, alternating currents, and vibration. Very few studies have attempted to develop such a model.

Batteries deployed in hybrid electric vehicles (HEV) are generally required to perform to specifications over an 8 year life cycle. In order to generate a more accurate model, the data of a battery system running at operating-mode conditions in a commercial HEV at Suzhou over a 1 year period was analyzed to determine the parameters for model. The resultant model, which does address the three parameters, is based on an analysis of these data and should therefore more closely reflect actual operating-mode performance.

In order to satisfy the commercial HEV requirement, we designed a newly high battery. The design ideas for the cell came from a fading reason analysis performed on the 8 Ah cell data gathered over 1 year. The simulation operating-mode model developed was then used to predict the performance of a newly designed high power battery.

2. METHOD

2.1 Battery and battery system introduced

The high power cells with an 8 Ah capacity which are nominally 8 mm thick, 134 mm wide, and 192 mm long were constructed using $LiNi_{0.4}Mn_{0.4}Co_{0.2}O_4$ (NCM, provided by 3M Tech. Co. Ltd., USA) as the cathode and artificial graphite (PSG-15, Changsha Xingcheng Co. Ltd., China) as the anode. The cathodes consisted of 90.5 wt% NCM, 3.5 wt% conductive black carbon, 1wt% Super-P, and 5 wt% polyvinylidene fluoride (PVDF). The anodes consisted of 94 wt% composite graphite, 4 wt% styrene–butadiene rubber, 1 wt% conductive black carbon, and 1 wt% carboxymethyl cellulose. The electrolyte was composed of a 1:1:1 volume ratio of ethylene carbonate (EC), ethyl-methyl carbonate (EMC), and dimethyl carbonate (DMC) with 1 M $LiPF_6$, using 2 wt% vinylene carbonate

(VC) as an additive. We constructed lamination-type batteries, using a UPZS40 (40 μm, UBE, Japan) separator and enclosed each battery in an aluminum plastic-laminated film box.

The battery system consisted of cells and a battery manager system (BMS), provided by EATON, USA. The total energy of the battery system was 5.5 kWh and the voltage 346 V. The battery system consisted of 192 high power 8Ah cells arranged as a 2 parallel and 96 series configuration (2P96S). The cell and the battery system are shown Fig.1. The state of charge (SOC) range of the battery system is used in the range 30% to 70% of capacity. The dimensions of the commercial HEV is 12000*2550*3250 (L*W*H) mm, and provided by Suzhou Kinglong Co. Ltd. (KLQ6129GQHEV). The commercial HEV were operated as buses in Suzhou, China.

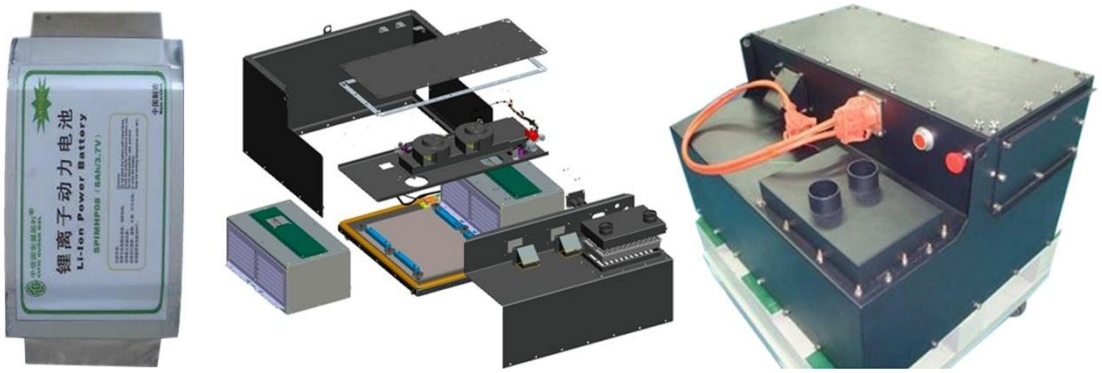

Figure 1. The photo of cell and battery system

The 6Ah cell chemistries designed for the experiment consisted of a positive electrode containing a partially substituted $LiNi_{0.4}Mn_{0.4}Co_{0.2}O_4$, and a negative electrode containing a pitch-based hard carbon. The cathodes consisted of 89.5 wt% NCM, 3.5 wt% conductive black carbon, 2 wt% Super-P, and 5 wt% PVDF. The anodes consisted of 90 wt% hard carbon, 8 wt% PVDF, 2 wt% conductive black carbon. The electrolyte was composed of a 2:3:5 volume ratio of ethylene carbonate (EC), ethyl-methyl carbonate (EMC), and dimethyl carbonate (DMC) with 1 M $LiPF_6$. We constructed lamination-type batteries, using a Celgard (25 μm, USA) separator and enclosed each battery in an aluminum plastic-laminated film box. The separator and electrolyte design was determined based on many experiments, the electrolyte being suitable for hard carbon and the separator having high porosity and low thickness.

2.2 Cell Characterization

The cells were tested by Arbin (Arbin Instruments, USA) at 2.75-4.2 V. The testing process included 0.3 C charge-discharge, hybrid pulse power characterization (HPPC), different rate charge-discharge and simulation operating-mode model testing. The objective of the HPPC test is to measure the discharge pulse and regeneration pulse power as functions of the depth of discharge (DOD). The rate of discharge pulse current is 5 C, and the rate of charge pulse current is 3.75 C. The discharge and regeneration DC resistances are calculated using a $\Delta V/\Delta I$ formula for each iteration of the test profile

in accordance with Fig.2, eqn. (1), and eqn. (2). The discharge and regeneration power are calculated with eqn. (3), and eqn. (4)[17].

Discharge Resistance $=\Delta V_{disc.}/\ \Delta I_{disc.}=（V_{T1}-V_{T0}）/（I_{T0}-I_{T1}）$ (1)

Regen Resistance $=\Delta V_{cha.}/\ \Delta I_{cha.}=（V_{T3}-V_{T2}）/（I_{T2}-I_{T3}）$ (2)

Discharge power= $V_{Min}（V_{T1}-V_{Min}）/ R_{dis}$ (3)

Regen power= $V_{Max}（V_{Max}-V_{T3}）/ R_{regen}$ (4)

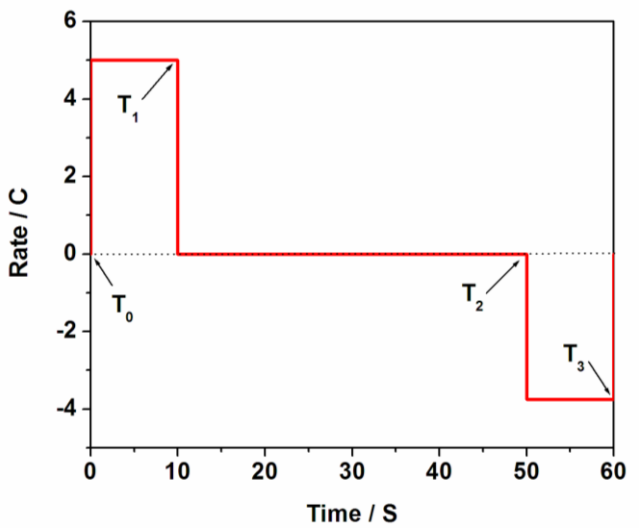

Figure 2. The HPPC testing procedure

The electrochemical impedance spectroscopy (EIS) was performed by a Zahner IM6e (Germany) electrochemical workstation, with a 5 mV AC perturbation over the frequency range from 0.1 Hz to 1,000 Hz at ambient conditions. The EIS was performed on the cells with the positive electrode as the working electrode and the negative electrode as both the reference and counter electrodes. The data of EIS were simulated by SIM soft, which is included in the Zahner IM6e electrochemical workstation.

The cells' performance, HPPC and EIS were all tested at 25℃

3. RESULTS AND DISCUSSION

3.1 Development of the simulation model based on an analysis of the data from the commercial HEV battery system

The data from the commercial HEV battery system was collected continuously over a period of 1 year. The times of collection numbers are 1341. The collection software captured 1 data point every 500 ms. To maximize the relevance of the collected data, samples were taken at various combinations of HEV operating state: accelerating, constant speed and deceleration. In total, the number of data captures was 341,239.

The data values captured were readings of current, voltage, temperature, power, capacity and time. The current values were rounded off to the nearest decade if the reading was greater than 5 A and to the nearest ampere if less than 5 A. The current value measured was the battery system current; the single cell's current is the system current value divided by two. The repetition frequency of the different currents after rounding is shown in Fig.3 and Tab.1.

Table 1. The appearing frequency of different current

Charge current / A	Frequency / n	Discharge current / A	Frequency / n
-250	0	0	0
-240	2	1	32320
-230	32	10	28721
-220	22	20	24796
-210	123	30	20231
-200	282	40	16131
-190	514	50	13944
-180	861	60	10482
-170	1127	70	8732
-160	1847	80	8412
-150	2531	90	6378
-140	2972	100	5042
-130	3696	110	4072
-120	4782	120	3018
-110	5957	130	2206
-100	7730	140	1507
-90	9298	150	1127
-80	10794	160	825
-70	11642	170	532
-60	12216	180	424
-50	11451	190	245
-40	11768	200	165
-30	14075	210	105
-20	11354	220	90
-10	11966	230	101
-1	14095	240	102
0	0	250	115
		260	86
		270	79
		280	69
		290	33
		300	12

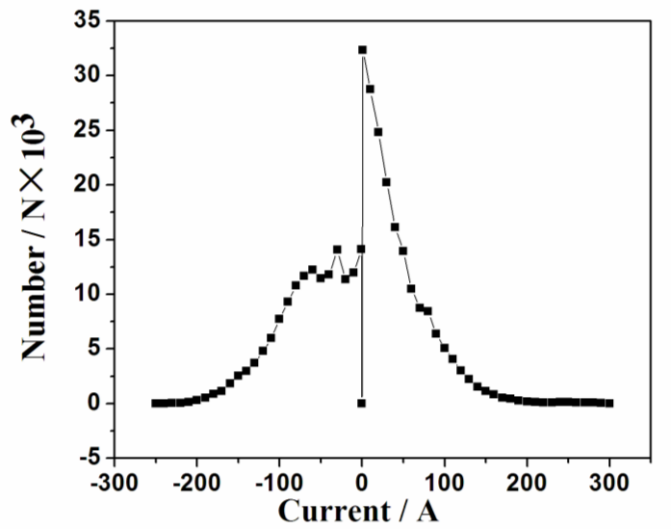

Figure 3. The appearing frequency of different current

From the data gathered, it was determined that the actual running current range of the battery system was between -240 A and 300 A. For a single cell, the discharge current fluctuated in the range 0-150 A, with about 92% being less than 50 A, and the peak at 150 A. In the regeneration recovery process, the current distribution was relatively wide, with approximately 84% between 0 and 50 A and approximately 97% between 0 and 75 A.The peak of the charge current was 120 A.

The model was subsequently developed by simulating the actual current data captured. The International Standards Organization (ISO) standard (ISO12405) was used as the simulating standard [18]. This simulation model only includes current changes. The operating-mode model is shown in Fig.4 and Tab.2. The SOC was increased by 2.5% at every charge mode iteration, and decreased by 2.5% at each discharge iteration. The charge and discharge iterations were 362 s and 349 s, respectively. The maximum charge current was 205.9 A, and the maximum discharge current was 237.7 A.

Table 2. The current data of operating-mode model: (a) Charge mode, (b) Discharge mode

(a) Charge mode					(b) Discharge mode				
Cumulative time / S	Step time /S	Current /A	Step SOC/%	Cumulative SOC/ %	Cumulative time / S	Step time /S	Current /A	Step SOC/%	Cumulative SOC/ %
1	1	-205.9	0.36	0.36	1	1	237.7	0.41	-0.41
8	7	-162.7	1.98	2.33	8	7	163.1	1.98	-2.39
33	25	-69	2.99	5.33	33	25	66.4	2.88	-5.28
66	33	-9.6	0.55	5.88	70	37	9.5	0.61	-5.89
76	10	0	0.00	5.88	80	10	0	0.00	-5.89
77	1	237.7	-0.41	5.47	81	1	-205.9	-0.36	-5.53
93	16	114.4	-3.18	2.29	97	16	-115.3	-3.20	-2.33

109	16	34.4	-0.96	1.33	113	16	-34.6	-0.96	-1.37
155	46	9.5	-0.76	0.57	153	40	-9.6	-0.67	-0.70
165	10	0	0.00	0.57	163	10	0	0.00	-0.70
190	25	-115.3	5.00	5.58	188	25	114.4	4.97	-5.66
220	30	-69	3.59	9.17	218	30	66.4	3.46	-9.12
240	20	34.4	-1.19	7.98	238	20	-34.6	-1.20	-7.92
268	28	66.4	-3.23	4.75	265	27	-69	-3.23	-4.69
271	3	163.1	-0.85	3.90	268	3	-162.7	-0.85	-3.84
276	5	0	0.00	3.90	273	5	0	0.00	-3.84
302	26	-34.6	1.56	5.46	299	26	34.4	1.55	-5.39
322	20	66.4	-2.31	3.16	319	20	-69	-2.40	-3.00
362	40	9.5	-0.66	2.50	349	30	-9.6	-0.50	-2.50

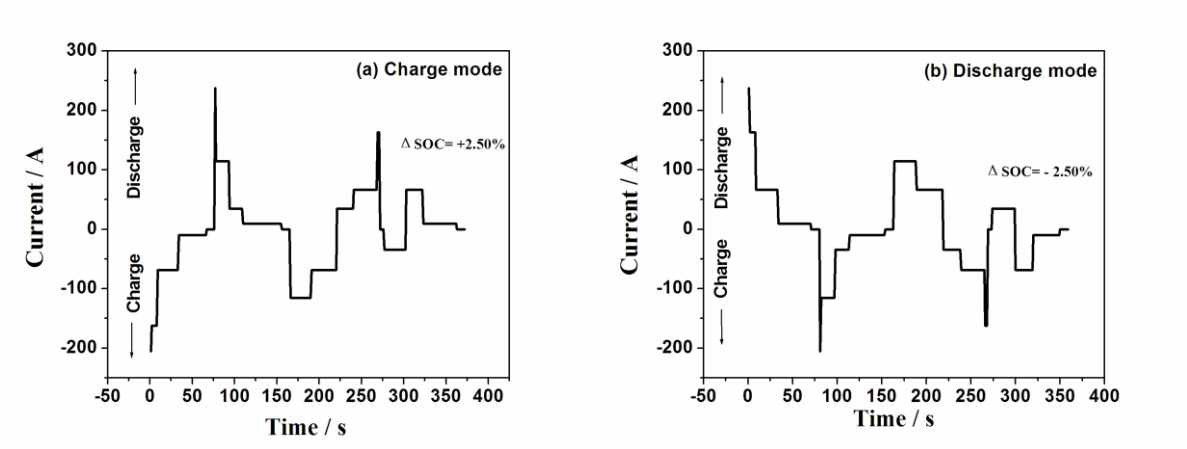

Figure 4. The current curve of operating-mode model: (a) Charge mode, (b) Discharge mode

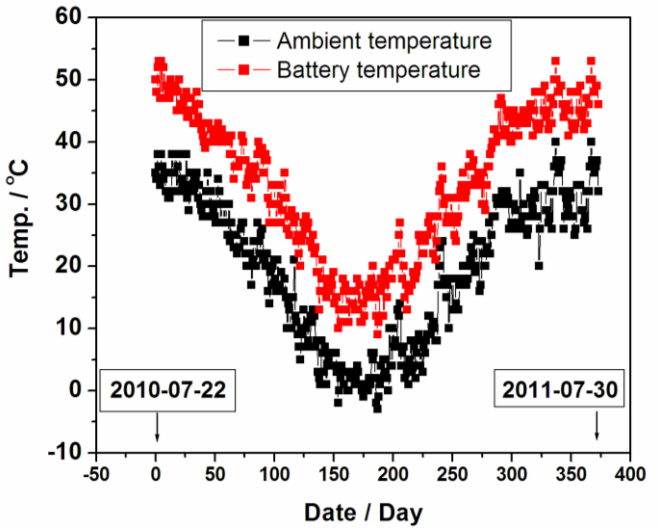

Figure 5. The temperature of ambient and battery within a year

The temperature data, also a major factor affecting the battery performance, is shown in Fig.5. The temperature of the battery was greater than ambient. The highest temperature of the battery was measured at 55 °C and the lowest temperature at 10 °C. The temperature variations simulated by the model were therefore chosen as 25 °C to 55 °C in 10 min, 180 min at 55 °C, 55 °C to 25 °C in 10 min, 210 min at 25 °C, 25 °C to 10 °C in 10 min, 240 min at 10 °C, 10 °C to 25 °C in 10 min, and 240 min at 25 °C.

The vibration is turbance was applied in an up-and-down motion at a frequency of 10-55 Hz with a peak acceleration of 30 ms^{-2}; this vibration mode was based on the established operating data for electric vehicles in Beijing, China [16].

By following this process a reliable model of the operating-mode conditions was established, which included the three important parameters of temperature, vibration, and current.

As a range of SOC from 30 to 70% is generally used for HEV, the simulation operating-mode model（SOM）procedure was determined to be as follows: battery charge stage from 30% to 70% SOC over a total of 12 charge mode cycles and an elapsed time of 4344 s; followed by a battery discharge stage from 70% to 30% SOC, over a total of 12 discharge mode cycles and an elapsed time of 4288 s; during the charge and discharge cycles the battery is simultaneously subjected to alternating temperature and vibration profiles.

3.2 Performance of the cell in a commercial HEV

Fig.6 shows the performance of the cell deployed in a commercial HEV. It illustrates that the resistance increases and the power decreases after a 1 year operating period and the discharge power decreases by 7.65% at 50% SOC. At the same time the discharge capacity is degraded with a capacity loss of approximately 3%. For the automotive industry, a battery life of 8 years is required. This generally means that the capacity loss and power loss must be less than 30% in 8 years. The 8 Ah battery does not meet these requirements.

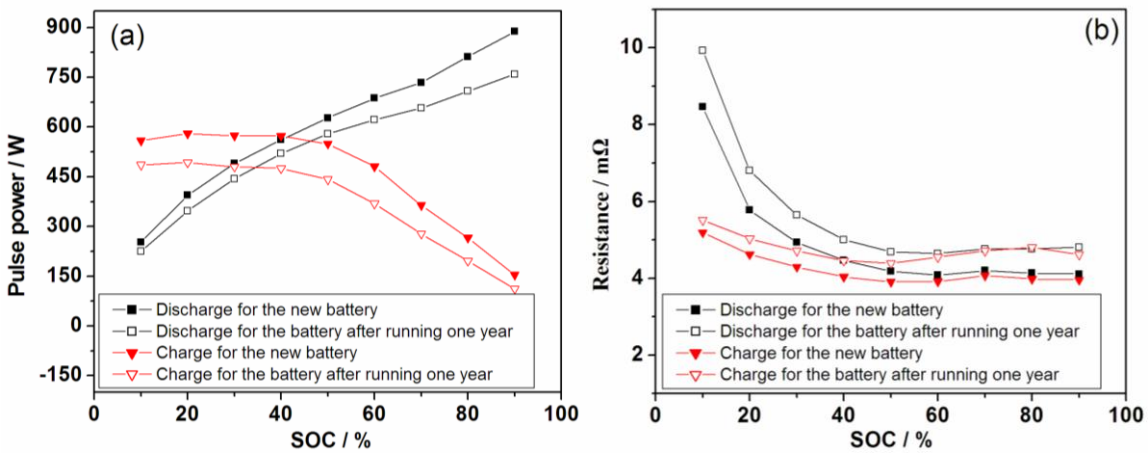

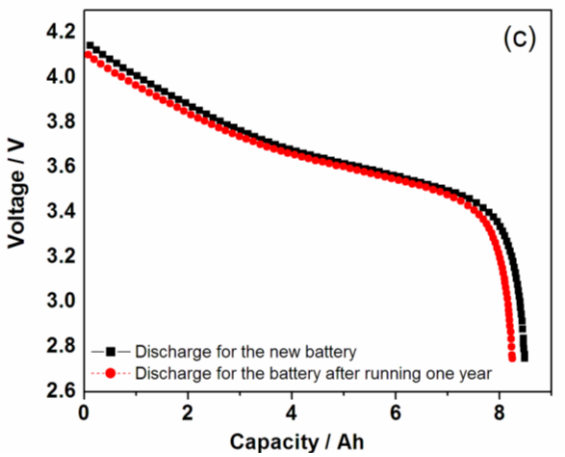

Figure 6. The performance of the cell working in commercial HEV, (a) power, (b) resistance, (c) capacity

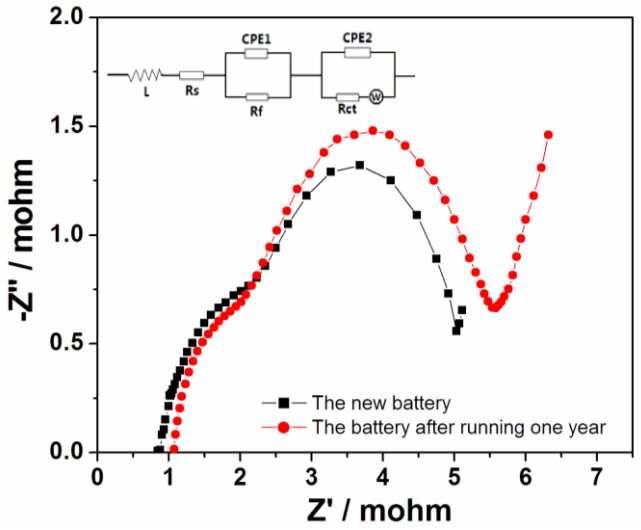

Figure 7. The EIS of battery before and after running

Table 3. The simulation date of battery before and after running

	R_s(mΩ)	R_f(mΩ)	R_{ct}(mΩ)
New cell	0.83	1.25	3.24
The cell after running one year	1.08	1.43	3.78

EIS is an effective method for analyzing the reasons for capacity and power degradation. Fig.7 shows the output from the EIS performed on the battery before and after operation. An equivalent circuit fitting was performed according to the literature [19-22]. According to the equivalent circuit, the EIS of the cells are composed of two partially overlapped and depressed semicircles at high to middle frequency and a slope line at low frequency. Inductance is represented by *L*. The intersection of

the diagram with the real axis refers to a bulk resistance, R_s, which reflects the electronic and ionic resistance of the electrodes and electrolyte/separator. CPE_1 and CPE_2 are the constant phase elements which were used instead of the capacitance, $C_{f,}$ of the solid electrolyte and double-layer capacitance, C_{dl}, respectively. The depressed semicircle at high frequency could be attributed to the resistance, R_f, and CPE_1. The depressed semicircle at the medium frequency could be attributed to the charge transfer resistance, R_{ct}, and CPE_2. The slope line at low frequency corresponds to the Warburg impedance, Z_w, which is related to the Li-ion diffusion within the particles [19-22].

Tab.3 shows the simulation data. The simulation determined that: R_f and R_{ct} increase significantly after actual operation for a year, as a result of the reaction from the SEI film repairing on the electrode surface between the electrolytes and active materials continued during the charge-discharge [16, 23]. After running at operating-mode conditions for 1 year, the surface membrane was severely damaged by the alternating temperatures combined with vibrations, which led to a more rapid repair of the surface membrane [16]. The current density is also an important factor, the battery suffered more than 120 A charge-discharge current, and the SEI film could be destroyed as a result of such a large current. The increase in R_s may be due to the reduction of electrode adhesion and the closing of the separator pore. The graphite will expand and contract because of temperature shock, vibration and large current charge-discharge, which will result in decreased adhesion of the negative electrode. As a result, the impedance increased more rapidly, with a consequent acceleration in capacity and power degradation.

3.3 Design of a new high power cell to satisfy the commercial HEV requirement

The design ideas for the cell came from a data analysis performed on the 8 Ah cell data gathered over 1 year. The resistance increase is a major contributing factor to the power and capacity degradation. The newly designed battery needed to address this.

The hard carbon materials have no graphitic structure; the layers of carbon atoms are not neatly stacked, are non-crystalline, and macroscopically isotropic. The spacing between planes of more than 0.38 nm means almost no volume change upon intercalation, and the structural exfoliation is not aroused by solvent intercalation. Also the electrochemical properties of hard carbon material are less sensitive to electrolyte compositions. Film-forming additives are not always necessary for hard carbon. The resistance of SEI film is very low or non-existent [24]. Therefore, the SEI film of a cell with hard carbon as the anode active material is not really affected by the alternating temperatures combined with vibration. The wider layer spacing of hard carbon is very beneficial for Li^+ de-intercalation. Hard carbon was chosen as the anode active material.

To reduce the effect of $R_{s,}$ which includes the electronic and ionic resistance of electrodes and electrolyte/separator, we increased the proportion of binder to improve the adhesion of the electrodes, and chose a separator with high porosity and low thickness [25].

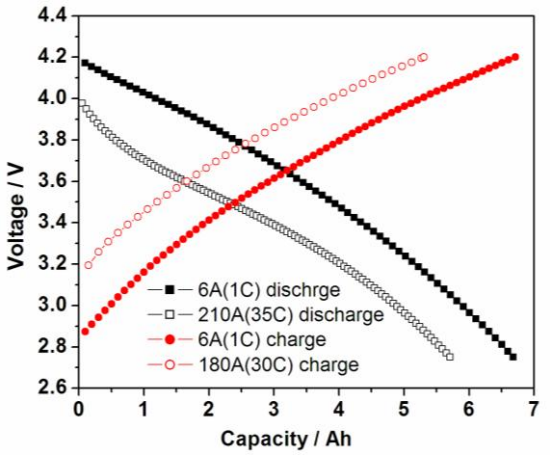

Figure 8. The performance of 6Ah battery

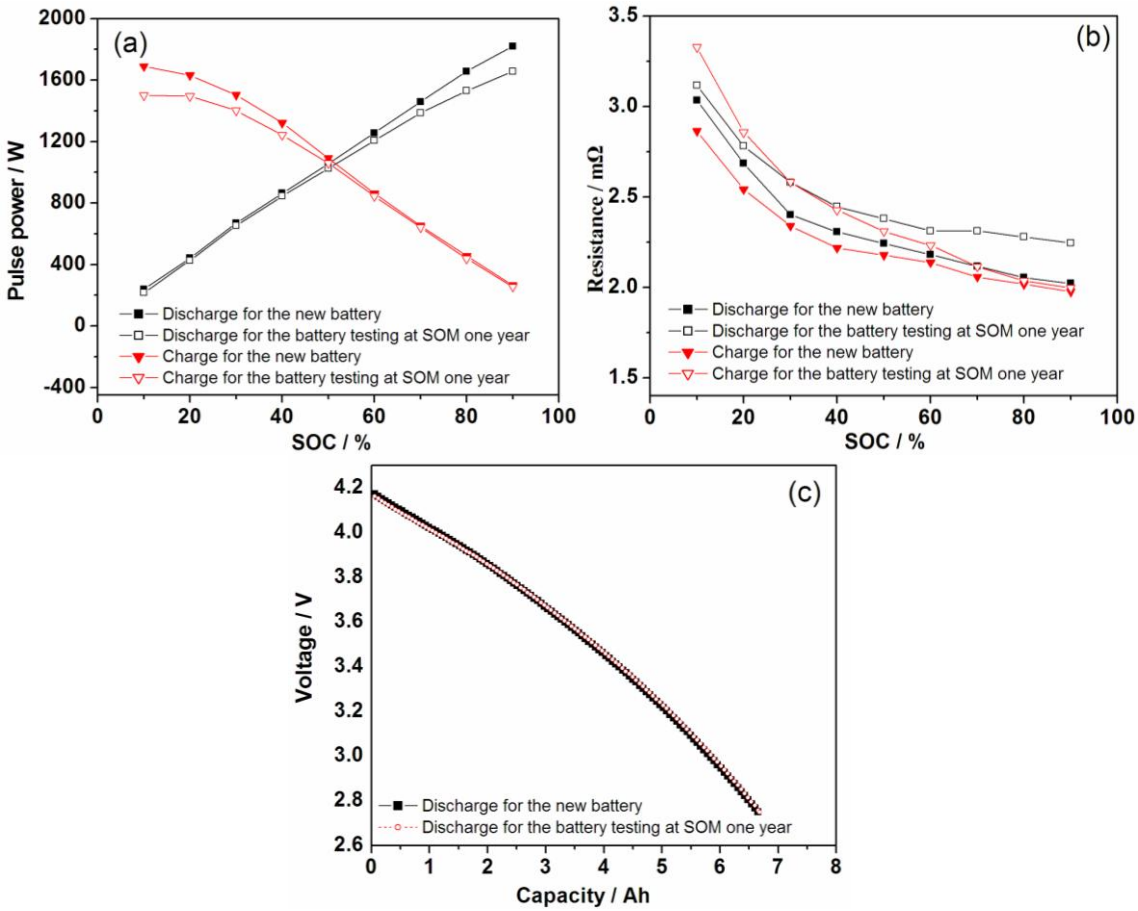

Figure 9. The testing of 6Ah battery at simulation operating-mode model (SOM), (a) power, (b) resistance, (c) capacity

After many experiments, the new high power battery was produced. Fig.8 shows the performance of the newly designed battery. The capacity of the battery is 6 Ah. The maximum charge

and discharge current reaches 180 A and 210 A, respectively. This current performance meets the requirements of commercial HEV applications.

The result of the 6 Ah battery 1-year simulations is shown in Fig.9. Compared to the actual 8 Ah cell running at operating-mode for 1-year, the 6 Ah cell displays little power loss and practically no degradation of capacity. The discharge power loss is less than 3% and the growth rate of resistance is only half of that for the 8 Ah at 50% SOC. The battery with hard carbon as the anode has no or very thin SEI film formation, and so the resistance is only marginally affected by temperature and vibration changes. The wider layer spacing can withstand rapid movement of Li^+ without damage to the surface film and changing volume. The increasing ratio of the PVDF-binder provides a high adhesive force for the electrode and reduces the bulk resistance after suffering thermal expansion, contraction, and vibration at SOM testing. The low increase in resistance maintains the power at relatively high levels. The 6 Ah high power battery therefore can meet the 8 year life cycle performance requirement of the automotive industry.

4. CONCLUSIONS

The commercial HEV with MGL's battery system were operated as buses in Suzhou, China. 341,239 data point captures from the battery system were made, via 1341 capture cycles over1 year. At operating-mode conditions, for the discharge current data, about 92% was less than 50 A, and the peak at 150 A; for the charge current, about 97% was less than 75A, and the peak at 120 A. A simulation model was developed which includes temperature shock, with current and vibration variations according to the ISO12405 standard. The model was based on collecting and studying the data from a commercial HEV battery system over a 1 year period. After running for 1 year, the resistance increased and the power decreased, and the discharge power decreased 7.65% at 50% SOC. At the same time the discharge capacity degraded with a capacity loss at about 3%. An EIS showed increasing resistance attributed to an increased SEI film thickness, and that the adhesion of the electrodes was reduced.

In order to meet the 8 year requirement of commercial HEV applications, a new cell of 6Ah was designed. The cell was designed with hard carbon as the anode, which has no or very thin SEI film, and so the resistance is not really impacted by temperature and vibration, and the wider layer spacing can withstand rapid movement of Li^+ without damaging the surface film and changing volume. Finally, the simulations run on the 6 Ah battery showed a maximum charge and discharge current reaching 180 A and 210 A, respectively. The discharge power loss was less than 3% and there was almost no degradation of capacity. It was therefore concluded that the 6Ah high power battery can meet the 8 year life cycle requirement of the automotive industry.

ACKNOWLEDGEMENTS
This work was supported by China 863 Science Foundation.

References

1. W. Waag, S. Käbitz, D. U. Sauer, *Applied Energy*, 102 (2013) 885-897.
2. N. Omar, M. A. Monem, Y. Firouz, J. Salminen, .J Smekens, O. Hegazy, H. Gaulous, G. Mulder, P. V. Bossche, T. Coosemans, .J V. Mierlo, *Applied Energy*, 113 (2014) 1575-1585.
3. Y. Xing, W. He, M. Pecht, K. L. Tsui, *Applied Energy*, 113 (2014) 106-115.
4. K. S. Ng, C-S Moo, Y. Chen, Y-C Hsieh, *Applied Energy*, 86 (2009) 1506-1511.
5. P. Ramadass, B. Haran, P.M. Gomadam, R. White, B.N. Popov, *J. Electrochem. Soc.*, 151 (2004) A196.
6. R. Spotnitz, *J. Power Sources*, 113 (2003) 72-80.
7. Á. G. Miranda, C. W. Hong, *Applied Energy*, 111 (2013) 681-689.
8. P. Tan, Z. Wei, W. Shyy, T. S. Zhao, *Applied Energy*, 109 (2013) 275-282.
9. C Hu, D Byeng, Youn, J Chung, *Applied Energy*, 92 (2012) 694-704.
10. M. Dubarry, B.Y. Liaw, *J. Power Sources*, 174 (2007) 856-860.
11. M. Safari, M. Morcrette, A. Teyssot, C. Delacourt, *J. Electrochem. Soc.*, 156 (2009) A145-A148.
12. Y. Xing, W. He, M. Pecht, K. L. Tsui, *Applied Energy*, 113 (2014) 106-115.
13. R. Darling, J. Newman, *J. Electrochem. Soc.*, 145 (1998) 990-998.
14. G. Ning, R.E. White, B.N. Popov, *Electrochim. Acta*, 51 (2006) 2012-2022.
15. J. Christensen, J. Newman, *J. Electrochem. Soc.*, 150 (2003) A1416.
16. N.N. Wu, D.J. Yang, J.H. Liu, W.H. Tian, *Electrochim. Acta*, 62 (2012) 91-96.
17. FreedomCAR Battery Test Manual for Power Assist Hybrid Electric Vehicles, U.S. Department of Energy, DOE/ID-11069, October 2003.
18. Electrically propelled road vehicles - Test specification for lithium-ion traction battery packs and systems - Part 2: High-energy applications ISO12405-2-2012.
19. F. Nobili, R. Tossici, F. Croce, B. Scrosati, R. Marassi, *J. Power Sources*, 94 (2001) 238-241.
20. B. Croce, F. Nobili, A. Deptula, W. Lada, R. Tossici, A. D'Epifanio, B. Scrosati, R. Marassi, *Electrochem. Commun.*, 1 (1999) 605-608.
21. M. Umeda, K. Dokko, Y. Fujita, M. Mohamedi, I. Uchida, J. Selman , *Electrochim. Acta*, 47 (2001) 885-890.
22. G. Fey, W.H. Yo, Y.C. Chang, *J. Power Sources*, 105 (2002) 82-86.
23. K. Xu, *Chem. Rev.*, 104 (2004) 4303-4417.
24. S. Flandrois, B. Simon, *Carbon*, 37 (1999) 165-180.
25. P. Arora, Z.M. Zhang, *Chem. Rev.*, 104 (2004) 4419-4462.